A constitutive model for ballistic gelatin at surgical strain rates

Nishant Ravikumar[a*], Christopher Noble[a*], Edward Cramphorn[a*] and Zeike A. Taylor[a]

[a] *CISTIB Centre for Computational Imaging and Simulation Technologies in Biomedicine, INSIGNEO Institute for in silico Medicine, Department of Mechanical Engineering, The University of Sheffield, Western Bank, Sheffield, S10 2TN, South Yorkshire, United Kingdom*

[*] *These authors contributed equally to this study.*

Corresponding author: Zeike A. Taylor, email: z.a.taylor@sheffield.ac.uk, telephone: +44 (0)114 2227719

Nishant Ravikumar, email: mt08nr@sheffield.ac.uk

Christopher Noble, email: mt08cn@sheffield.ac.uk

Edward Cramphorn, email: e.cramphorn@sheffield.ac.uk

Abstract

This paper describes a constitutive model for ballistic gelatin at the low strain rates experienced, for example, by soft tissues during surgery. While this material is most commonly associated with high speed projectile penetration and impact investigations, it has also been used extensively as a soft tissue simulant in validation studies for surgical technologies (e.g. surgical simulation and guidance systems), for which loading speeds and the corresponding mechanical response of the material are quite different. We conducted mechanical compression experiments on gelatin specimens at strain rates spanning two orders of magnitude ($\sim 0.001 - 0.1s^{-1}$) and observed a nonlinear load-displacement history and strong strain rate-dependence. A compact and efficient visco-hyperelastic constitutive model was then formulated and found to fit the experimental data well. An Ogden type strain energy density function was employed for the elastic component. A single Prony exponential term was found to be adequate to capture the observed rate-dependence of the response over multiple strain rates. The model lends itself to immediate use within many commercial finite element packages.

Keywords:
Ballistic gelatin, constitutive model, uni-axial compression, mechanical characterisation, quasi-static strain rates, visco-hyperelasticity

1. Introduction

In this paper we propose a constitutive modelling framework for ballistic gelatin at low (quasi-static) strain rates. Based on observed experimental results (both here and in previous studies), we aim in particular to capture the strong strain rate-dependence of the material, which is not possible with elastic models only. A combined experimental and analytical approach is used to determine a suitable form for the constitutive equations. Experiments

and models are then linked via a parameter fitting routine that combines an optimisation algorithm with a computational model of compression experiments.

Organically-derived gels, hydrogels, silicon-gels, etc. have been used in a variety of biomedical applications (Juliano et al. (2006); Trexler et al. (2011); Drury and Mooney (2003); Sun et al. (2012); Pervin and Chen (2011)). Soft tissue substitutes like these are favoured over native soft tissue for many applications due to the ease of sourcing such materials, the ability to control the sample preparation processes (e.g. composition and shape), and ethical implications. Ballistic gelatin in particular has frequently been employed as a soft tissue substitute (Kwartowitz (2012); Malekzadeh et al. (2011); Mendez-Probst et al. (2010)) as it is biologically-derived and has favourable properties such as biodegradability and ease of manufacture and preparation. Moreover, its mechanical properties and response to a variety of mechanical tests have been found to be similar to those of soft tissues (Breeze et al. (2013); Kalcioglu et al. (2010)), further enhancing its suitability as a substitute. Its primary use has been in forensic and military applications (Liu et al. (2014a)), most notably ballistic impact (Alley et al. (2011)), wound profiling, and projectile wounding/penetration studies (Liu et al. (2014b); Swain et al. (2014)). But, it has also found important application as a phantom material in medical imaging and surgical-guidance studies (e.g. simulating breast, prostate and other tissues) (Lawrentschuk et al. (2011); Lindner et al. (2010); Maier-Hein et al. (2009); Miranda et al. (2013); März et al. (2014); Sutcliffe et al. (2013)), wherein it has been found to emulate soft tissue properties with satisfactory fidelity. It is these latter applications, in which loading speeds (that we loosely call 'surgical speeds') are several orders of magnitude lower than in ballistics studies, that motivate the present work. In this context, availability of a reliable constitutive model will allow in silico simulation of experimental scenarios to be undertaken, and correlated with experimental observations themselves.

This study is concerned with modelling the time- and rate-dependence of the gelatin's mechanical response at quasi-static loading speeds. The majority of past studies have focused on characterisation at 'dynamic' ($\sim 1000 - 3000 s^{-1}$) strain rates, reflecting its primary application area (Kwon and Subhash (2010); Subhash et al. (2012); Salisbury and Cronin (2009)). Test configurations such as Hopkinson bar impact (Cronin and Falzon (2009)), uniaxial tension (Moy et al. (2008)), indentation (Juliano et al. (2006)), and others have been used for this purpose. But, it is widely recognised that the material's constitutive behaviour is distinctly different under these two loading speed regimes, possibly due to microstructural re-organisation of the material at higher rates (Kwon and Subhash (2010)). Typically, the material appears much stiffer at higher speeds, though rate-dependence can indeed be observed across all speeds studied so far. As a result it is difficult to formulate general constitutive models that capture the gelatin response at *both* quasi-static and dynamic loading rates, nor indeed may this be an efficient approach if only a narrow envelope of speeds is of interest in any single application.

Characterisation at lower speeds, similar to here, was considered in (Cronin and Falzon (2011); Cronin (2011)). Both finite strain behaviour and strain rate-dependence were studied. In (Cronin and Falzon (2011)), compression tests at various loading speeds were performed and the responses were modelled with a simple Neo-Hookean type hyperelastic constitutive model. Such models, however, are unable to capture strain rate-dependence, and it was therefore separately fit to the data for each strain rate. Improved models aimed at addressing this deficiency were proposed in (Cronin (2011)) in the form of quasi-linear viscoelasticity and

tabulated hyperelasticity, both of which are able to capture strain rate-dependence, though using quite different approaches. Viscoelastic models are formulated in terms of a convolution integral that imbues a dependence on the entire strain history of the material, naturally including, for example, temporal patterns of strain magnitude and rate. This is coupled with relaxation functions, usually of exponential decay form, that reflect viscous phenomena. Many important physical manifestations of these mechanisms, such as stress relaxation, creep and rate-dependence therefore naturally emerge from such models. In contrast, tabulated models, which were favoured in (Cronin (2011)), simply incorporate an ensemble of elastic response curves at different strain rates, and provide a numerical mechanism for switching between them according to the imposed loading characteristics (Kolling et al. (2007)). The approach is general in the sense that quite varied phenomena can be included (for example, a wide range of loading speeds was considered in (Cronin (2011)), as well as material damage), but it relies on provision of a sufficiently rich set of constituent curves to cover the desired range of loading conditions. Instabilities may also be introduced when transitioning between certain loading regimes, meaning additional care must be taken in those regions (Kolling et al. (2007)).

In this work, we revisit the viscoelastic approach, which, though more complex in its functional form, offers a more compact overall representation of the key response features. It also provides a continuous and smooth prediction of mechanical response across its range of validity. We couple the basic viscoelastic formulation with a suitable hyperelastic strain energy function to accommodate not only the time- and rate-dependence, but finite deformation features also. The resulting model can be efficiently solved in any finite element (FE) framework. Compression testing of cylindrical gelatin specimens at a range of loading speeds was also undertaken, on the basis of whose results suitable model parameters for this material were identified. A curve fitting scheme based on a FE model of the compression experiments was developed for this purpose. Finally, a sensitivity analysis on the model parameters was conducted to gauge the reliability of the obtained parameter values. The resulting model is suitable for use in simulated surgical scenarios, as described, in which ballistic gelatin is used as a soft tissue surrogate.

2. Mechanical Testing

2.1. Sample preparation

Gelita Type 3 scientific grade ballistic gelatin[1] was selected for this study due to its high thermal and chemical stability, which serves to maximise repeatability in the mechanical tests. The base material is produced from denatured porcine collagen that is also treated and stabilised to improve lifespan and reduce fungal and bacterial growth. In final form, it is soft and transparent with a yellow tinge. It is supplied as a dry powder, which affords control over the concentration and volume of the final gelatin material. All ballistic gelatin samples used in this study were produced to a concentration of 10% weight/volume (w/v) in water, reflecting the practice in previous studies (Cronin and Falzon (2011); Detwiler et al. (1991); Nicholas and Welsch (2004); Richler and Rittel (2014)). The powder was mixed with cold

[1]URL: www.gelita.com

water to the desired concentration and volume and left to hydrate for 24 hours. The mixture was then heated to 50±5°C in a water bath to allow dissolution, and any scum that formed was skimmed off till the gelatin was free of air bubbles and had a uniform consistency. This helped to minimise variations in the surface properties of the samples. The liquid gelatin was poured into a casting mould to a height of 10 mm and left to solidify for 24 hours (see Fig. 1), before being removed, wrapped in plastic to prevent dehydration, and left to cure for 24 hours in a fridge. Subsequently, it was cut into 30 mm diameter cylindrical samples for testing (see Fig. 2). Markers were positioned in the mould to allow a consistent cast sheet thickness (and sample height) of 10 mm to be produced. Casting the gelatin as sheets also allowed samples to be cut from the central region, thereby avoiding meniscus effects near the edges. Care was taken during cutting to minimise production of surface and edge artefacts in the samples. Any samples showing imperfections considered detrimental to the mechanical response were discarded. The compliance of the gelatin itself also meant it deformed slightly during cutting, so that the resulting specimens were likely slightly non-cylindrical. However, the effect was in all cases small, and usually undetectable. Two batches of material were independently produced for testing on separate days. Each batch yielded nine cylindrical specimens, three of which were tested at each of the three loading rates (see Sec. 2.2).

Figure 1: Liquid gelatin cast into the mould after dissolving the gelatin powder in water. Scum is visible on the top layer of the material.

2.2. Uni-axial Compression Tests

Compression tests were performed using a Bose ElectroForce (3200 system) mechanical testing machine with a 450 N load cell. The cylindrical samples were mounted between two flat plates (Fig. 3) and a pre-load of 1 N was applied to ensure good contact between sample and plates. Samples were compressed by 25% of their initial height. Three compression rates were employed: 1 mm/s (fast), 0.1 mm/s (intermediate) and 0.01 mm/s (slow), correspond-

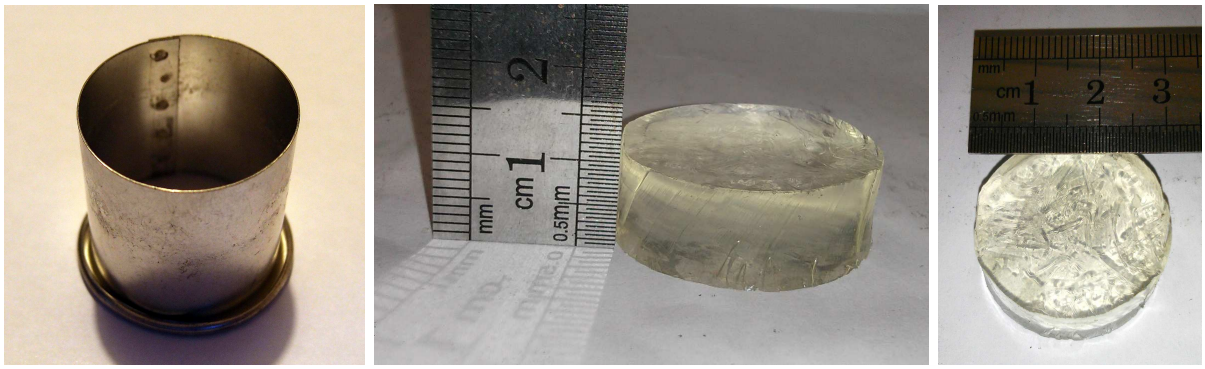

Figure 2: The cylindrical cutting instrument used during sample preparation (left), and resulting test specimens of 30 mm diameter and 10 mm height (middle and right).

ing to nominal[2] strain rates of 0.1, 0.01 and 0.001 s^{-1}, respectively. Initial investigations showed that the response of the gelatin was sensitive to temperature (see also Cronin and Falzon (2011)). All samples were therefore refrigerated up to the point of testing to minimise variation due to thermal effects.

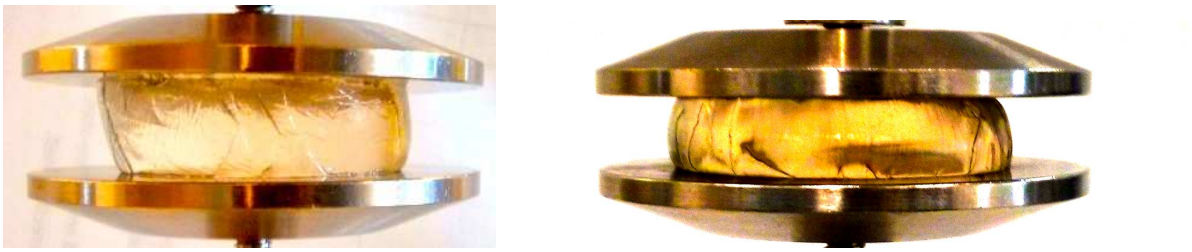

Figure 3: Left: a gelatin sample held between the load plates of the mechanical testing device with pre-load of 1 N applied prior to compression. Right: a second sample at 25% compression.

As shown in Fig. 3, adherence of the gelatin to the load plates means the specimens deformed non-uniformly under compression. To a close approximation, this represents a 'no-slip' condition at the sample-plate interfaces. An alternative approach is to attempt to minimise friction at these interfaces (for example by lubricating) so that the specimens can expand approximately uniformly. The main advantage of such a configuration is availability of closed form expressions relating compression level to reaction force, which then afford simple fitting of constitutive models to the experimental results by means of an optimisation procedure. The disadvantage, however, is uncertainty in the level of interface friction that inevitably remains, which imparts to the fitted model parameters an uncertain amount of error. In the present experiments, therefore, a no-slip condition was imposed, thereby removing the ambiguity of the interface conditions. Since no analytical solutions are available for this non-uniform deformation problem, we employed FE-based solution in our parameter

[2]These are not, in general, the actual strain rates within the material, since the specimen deformation is non-uniform; we use the term nominal to mean 'change in specimen height divided by original height'

fitting routine (see Sec. 3.4).

2.3. Experimental Results

The mean force-displacement curves (averaged across all specimens) for each loading rate are shown in Fig. 4. The strong load rate-dependence of the response is clearly evident, with higher speeds producing higher stiffness. Some nonlinearity with the displacement level (i.e. stiffening) can also be seen. As indicated by the relatively small standard deviations, the inter-specimen variability was low. Though it is not revealed in the plots shown here, the inter-batch (i.e. across independently produced gelatin batches) variability was somewhat higher than the intra-batch variability, which perhaps can be attributed to slight variations in the sample preparation conditions on each day. In particular, dissolution and mixing of the gelatin in its initial powdered form can lead to localised regions of high concentration, to which the mechanical response may be sensitive. Nonetheless, the low overall variability shown in Fig. 4 indicates good overall repeatability in the preparation process.

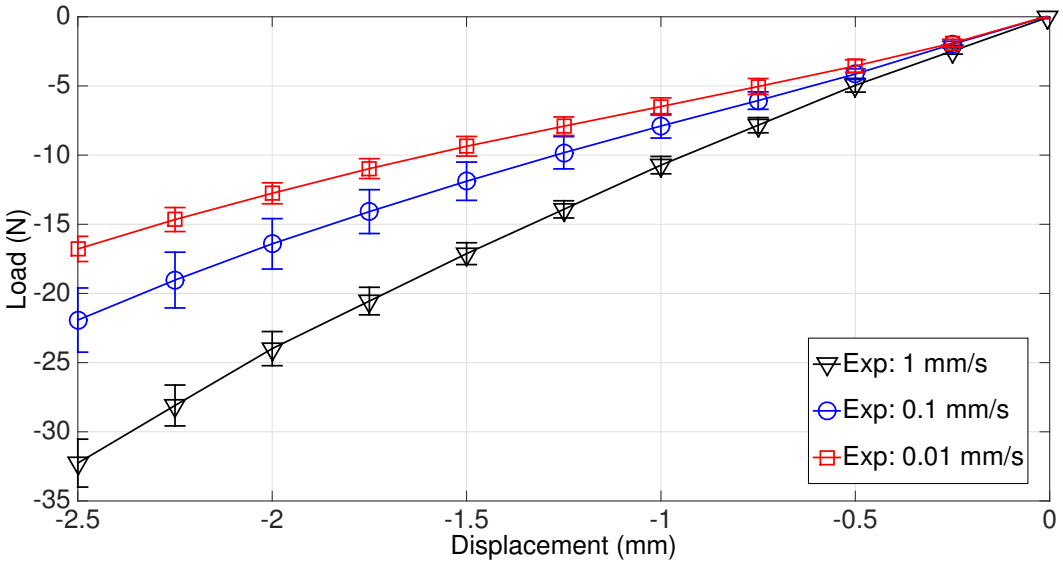

Figure 4: Mean load-displacement data (averaged over all specimens) for each of the three load rates. Error bars denote ±1 standard deviation.

3. Constitutive Modelling

Motivated by the strong load rate-dependence observed in the experimental results, and by the nonlinearity of the individual curves, we propose a visco-hyperelastic constitutive model which combines large strain capabilities with so-called load history-dependence. The flexibility of this approach allows a single model (i.e. with a single set of parameters) to capture the response across all three loading rates, making it suitable for diverse applications. For these reasons, models of this type have indeed been applied to various soft tissues, also, such as liver (Samur et al. (2007)) and brain (Miller and Chinzei (2002)). In the following, we briefly introduce essential quantities for describing motion of a continuum body (kinematics),

before reviewing the general form of this model class, and finally describing the particular formulation proposed for gelatin. Further details of the underlying solid continuum mechanics can be obtained from texts such as (Holzapfel (2000)). Bold variables are used to indicate vector and tensor quantities.

3.1. Kinematics

A deformable body is considered to have an undeformed, stress-free configuration (called its reference configuration) prior to application of any loads, and a deformed configuration at any time afterwards (called its current configuration). Let $\mathbf{X}$ and $\mathbf{x}$ be the reference and current coordinates of a given particle in this body, so that the particle's displacement is given by $\mathbf{u} = \mathbf{x} - \mathbf{X}$. These coordinates are also assumed to be related through $\mathbf{x} = \chi(\mathbf{X})$ where χ represents the deformation field expressed in the reference configuration. Starting from these definitions, various measures of relative deformation and strain can be defined, beginning with the deformation gradient tensor, which describes stretches and rotations of differential material fibres at this point, and is given by (Holzapfel (2000)):

$$\mathbf{F} = \frac{\partial \mathbf{x}}{\partial \mathbf{X}}. \tag{1}$$

In a Lagrangian description, as used here, the right Cauchy-Green deformation and Green-Lagrange strain tensors will be of use and are given, respectively, by (Holzapfel (2000)):

$$\mathbf{C} = \mathbf{F}^T\mathbf{F}, \tag{2}$$

$$\mathbf{E} = \frac{1}{2}\left(\mathbf{C} - \mathbf{I}\right). \tag{3}$$

If we define the stretch λ as the relative change in length of a material fibre along some direction $\mathbf{n}$, it can be shown that

$$\lambda^2 = \mathbf{n} \cdot \mathbf{C}\mathbf{n}. \tag{4}$$

Thus, $\mathbf{C}$ describes the stretching in any direction undergone by material fibres. If $\mathbf{n}$ represents the a^{th} principal direction for the current deformation state, then the corresponding λ_a is called the a^{th} principal stretch. In three dimensions, there will be three principal stretches.

In the case of nearly-incompressible materials, it is often convenient to split the deformation gradient $\mathbf{F}$ into isochoric (volume preserving) and volumetric components (Holzapfel (2000)), resulting in:

$$\mathbf{F} = J^{1/3}\bar{\mathbf{F}} \tag{5a}$$

$$\bar{\mathbf{C}} = \bar{\mathbf{F}}^T\bar{\mathbf{F}} = J^{2/3}\mathbf{C} \tag{5b}$$

$$\bar{\lambda}_a = J^{-1/3}\lambda_a, \quad a = 1, 2, 3 \tag{5c}$$

Here, $J = \det \mathbf{F}$ is the Jacobian determinant, which represents the volume change in the material, $\bar{\mathbf{F}}$ and $J^{1/3}$ are the isochoric and volumetric parts of the deformation gradient, $\bar{\mathbf{C}}$ is the modified right Cauchy-Green deformation tensor, and $\bar{\lambda}_a$ are the corresponding modified principal stretches. These kinematic quantities are the building blocks on which hyperelastic (or, in this case, visco-hyperelastic) constitutive models are developed.

3.2. Visco-hyperelastic constitutive equations

Our constitutive model is formulated in terms of a Helmholtz free energy function W, which captures the stored elastic energy associated with the current state of deformation, minus the effects of dissipation over the history of the deformation (Holzapfel (2000)). It is thus a function both of the current deformation and of time. Using the isochoric/volumetric split of the deformation gradient described above, W, too, can be expressed as a combination of isochoric W_{iso} and volumetric W_{vol} components. We assume that dissipitive mechanisms affect only the isochoric components, and that the material remains almost incompressible. So, in general:

$$W(\bar{\lambda}_1, \bar{\lambda}_2, \bar{\lambda}_3, J, t) = W_{iso}(\bar{\lambda}_1, \bar{\lambda}_2, \bar{\lambda}_3, t) + W_{vol}(J) \tag{6}$$

where

$$W_{iso}(\bar{\lambda}_1, \bar{\lambda}_2, \bar{\lambda}_3, t) = \int_0^t \phi(t-s) \frac{\mathrm{d}W_{iso}^E(\bar{\lambda}_1, \bar{\lambda}_2, \bar{\lambda}_3)}{\mathrm{d}\tau} \, \mathrm{d}s \tag{7}$$

and $W_{vol}(J)$ are isochoric and volumetric terms, respectively, $W_{iso}^E(\bar{\lambda}_1, \bar{\lambda}_2, \bar{\lambda}_3)$ is the underlying elastic response of the isochoric component, and

$$\phi(t) = \phi_\infty + \sum_{i=1}^{N^\phi} \phi_i \, e^{-t/\tau_i} \tag{8}$$

is a relaxation function expressed in Prony series form with N^ϕ terms.. The convolution integral in (7) imparts the loading history-dependence mentioned above. τ_i are relaxation time constants, which control the rate of stress relaxation in the material (i.e. higher values mean slower relaxation). ϕ_∞ and ϕ_i are equilibrium and relaxation moduli, respectively, constrained according to $\phi_\infty + \sum_i \phi_i = 1$. This commonly used Prony series representation has a physical analogue in the form of a generalised Maxwell viscoelastic solid with N^ϕ spring-dashpot elements in parallel (Holzapfel (1996); Roylance (2001)), and a final parallel spring that controls the equilibrium behaviour. Such a formulation can account for dissipative effects that manifest as load rate-dependence, creep and stress relaxation, and its inclusion imbues our model, too, with strain rate-dependence. Such a model also lends itself to efficient numerical solution within a FE context (Taylor et al. (2009)) and is therefore often used in commercial FE packages. We found that using $N^\phi = 1$ was sufficient to capture the load rate-dependence observed in the experimental results.

Given a free energy function W, the second Piola-Kirchhoff stress $\mathbf{S}$ can be obtained from $\mathbf{S} = \partial W / \partial \mathbf{E} = 2 \partial W / \partial \mathbf{C}$ (Holzapfel (2000)). If W is split as in (6), the stress can be similarly split, and written as:

$$\mathbf{S}(\bar{\lambda}_1, \bar{\lambda}_2, \bar{\lambda}_3, J, t) = \mathbf{S}_{iso}(\bar{\lambda}_1, \bar{\lambda}_2, \bar{\lambda}_3, t) + \mathbf{S}_{vol}(J), \tag{9}$$

where

$$\mathbf{S}_{iso} = 2 \frac{\partial W_{iso}(\bar{\lambda}_1, \bar{\lambda}_2, \bar{\lambda}_3, t)}{\partial \mathbf{C}} = \int_0^t \phi(t-s) \frac{\mathrm{d}}{\mathrm{d}s} 2 \frac{\partial W_{iso}^E(\bar{\lambda}_1, \bar{\lambda}_2, \bar{\lambda}_3)}{\partial \mathbf{C}} \, \mathrm{d}s \tag{10}$$

and

$$\mathbf{S}_{vol} = 2 \frac{\partial W_{vol}(J)}{\partial \mathbf{C}} = J \frac{\mathrm{d}W_{vol}(J)}{\mathrm{d}J} \mathbf{C}^{-1} \tag{11}$$

are isochoric and volumetric components of $\mathbf{S}$. The elastic isochoric term $2\partial W^E_{iso}/\partial \mathbf{C}$ in (10) is a symmetric second order tensor, representing a stress-like quantity. Any such tensor $\mathbf{A}$ has a spectral representation in terms of its eigenvalues A_a and unit eigenvectors $\hat{\mathbf{n}}_a$ $(a = 1, 2, 3)$: $\mathbf{A} = \sum_{a=1}^{3} A_a \hat{\mathbf{n}}_a \otimes \hat{\mathbf{n}}_a$, and these A_a and $\hat{\mathbf{n}}_a$ can be recognised as the tensor's principal values and directions. Using this identity, and some algebraic manipulation, the elastic isochoric term can be further expanded as

$$\begin{aligned} 2\frac{\partial W^E_{iso}}{\partial \mathbf{C}} &= \sum_{a=1}^{3} \frac{1}{\lambda_a} \frac{\partial W^E_{iso}}{\partial \lambda_a} \hat{\mathbf{n}}_a \otimes \hat{\mathbf{n}}_a, \\ &= \sum_{a=1}^{3} \frac{1}{\lambda_a^2} \left(\bar{\lambda}_a \frac{\partial W^E_{iso}}{\partial \bar{\lambda}_a} - \frac{1}{3} \sum_{b=1}^{3} \bar{\lambda}_b \frac{\partial W^E_{iso}}{\partial \bar{\lambda}_b} \right) \hat{\mathbf{n}}_a \otimes \hat{\mathbf{n}}_a, \end{aligned} \tag{12}$$

where the dependence of W^E_{iso} on $\bar{\lambda}_a$ has been omitted for brevity. (See Holzapfel (2000) for further details).

3.3. Particular forms of the strain energy terms

Particularisation of the constitutive model for the gelatin requires specification of the forms of the elastic isochoric and volumetric strain energy terms. We propose an Ogden hyperelastic model, in which

$$W^E_{iso}(\bar{\lambda}_1, \bar{\lambda}_2, \bar{\lambda}_3) = \sum_{i=1}^{N^H} \frac{\mu_i}{\alpha_i^2} \left(\bar{\lambda}_1^{\alpha_i} + \bar{\lambda}_2^{\alpha_i} + \bar{\lambda}_3^{\alpha_i} - 3 \right), \tag{13}$$

and

$$W_{vol}(J) = \frac{\kappa_0}{2}(J-1)^2. \tag{14}$$

Here, μ_i and α_i $(i = 1, \ldots, N^H)$ are shear moduli and dimensionless constants, respectively, and N^H is the number of terms in the series. The parameters μ_i and α_i are related to the initial shear modulus μ_0 via $2\mu_0 = \sum_{i=1}^{N^H} \alpha_i \mu_i$. κ_0 is the initial bulk modulus, which we here approximate as $\kappa_0 = 2\mu_0(1+\nu)/3(1-2\nu)$, with an assumption that Poisson's ratio $\nu = 0.49$, representing near incompressibility.

We found that $N^H = 1$ term was sufficient to capture well the observed gelatin response. Several simpler forms were considered, in particular the neo-Hookean and two-parameter Mooney-Rivlin models (both of which are in fact special cases of (13)-(14)), as well as more complex models with $N^H > 1$. However, we concluded that a single-term Ogden model, involving just two parameters (μ_1 and α_1), offered the best balance between computational complexity and quality of fit to the experimental curves.

The complete model may be implemented within many commercial FE packages. In this work, we employed Abaqus[3], which represents the relaxation function $\phi(t)$ in slightly modified form:

[3]URL: http://www.3ds.com/products-services/simulia/portfolio/abaqus/overview/

$$\phi(t) = \mu_0 \left(\gamma_\infty + \gamma_1 \, e^{-t/\tau_1}\right), \tag{15}$$

where $\gamma_1 = \phi_1/\mu_0$ and $\gamma_\infty = \phi_\infty/\mu_0$. The model therefore has four independent parameters that must be specified based on the experimental results in Sect. 2: μ_1, α_1, γ_1 and τ_1.

3.4. Model parameter estimation

As noted, in the absence of analytical expressions for the load-displacement relationship in our experimental configuration, we employed FE solution to generate load-displacement curves for given material parameters. Here follows a description of the computational model and the optimisation scheme in which it was used.

3.4.1. Finite element analysis of the compression experiment

FE solution of the compression problem using the constitutive model formulated above was obtained with an axisymmetric model comprising 1500 4-node quadrilateral elements (Abaqus element type CAX4R), the validity of which mesh density was assessed via a mesh independence study. The plates were represented as rigid bodies that contact and deform the gelatin specimen. Tie constraints were also used at the specimen-plate interface to enforce the no-slip condition. Fully non-linear, large deformation analysis was used. The initial model configuration and an example deformed result are shown in Fig. 5.

3.4.2. Global optimisation

The model fitting process was formulated as a least squares optimisation problem, minimising the difference between mean experimental (Fig. 4) and model-predicted reaction force histories ($\mathbf{F}_{\text{exp}}$ and $\mathbf{F}_{\text{mod}}$, respectively):

$$\mathbf{x} = \arg\min_{\mathbf{x}} \|\mathbf{F}_{\text{exp}} - \mathbf{F}_{\text{mod}}\|_2, \tag{16}$$

where $\mathbf{x} = \{\mu_1, \alpha_1, \gamma_1, \tau_1\}$ are model parameters. The model was fit to data from the three loading rates simultaneously by concatenating these within $\mathbf{F}_{\text{exp}}$ and $\mathbf{F}_{\text{mod}}$. Eqn. (16) was solved using the 'trust region reflective' (TRR) algorithm within Matlab's[4] 'lsqnonlin' function, which was found to perform well for this problem. In each iteration of the optimiser, $\mathbf{F}_{\text{mod}}$ was evaluated using the FE model described above. A similar approach was devised in (Taylor et al. (2007)). Three complete simulations were performed in each iteration, yielding the required results for the three loading rates. Upper and lower bounds were imposed on the model parameters to limit the search space of the optimiser and ensure physical plausibility. The entire procedure was executed within a multi-start wrapper to avoid the danger of optimisation towards local minima. Finally, we note that a single fitting to the averaged experimental data from all samples was performed. An alternative approach is to fit separately to each experimental curve and average the resulting parameters, but see the discussion of this point in (Robertson and Cook (2014)).

[4]URL: www.mathworks.com

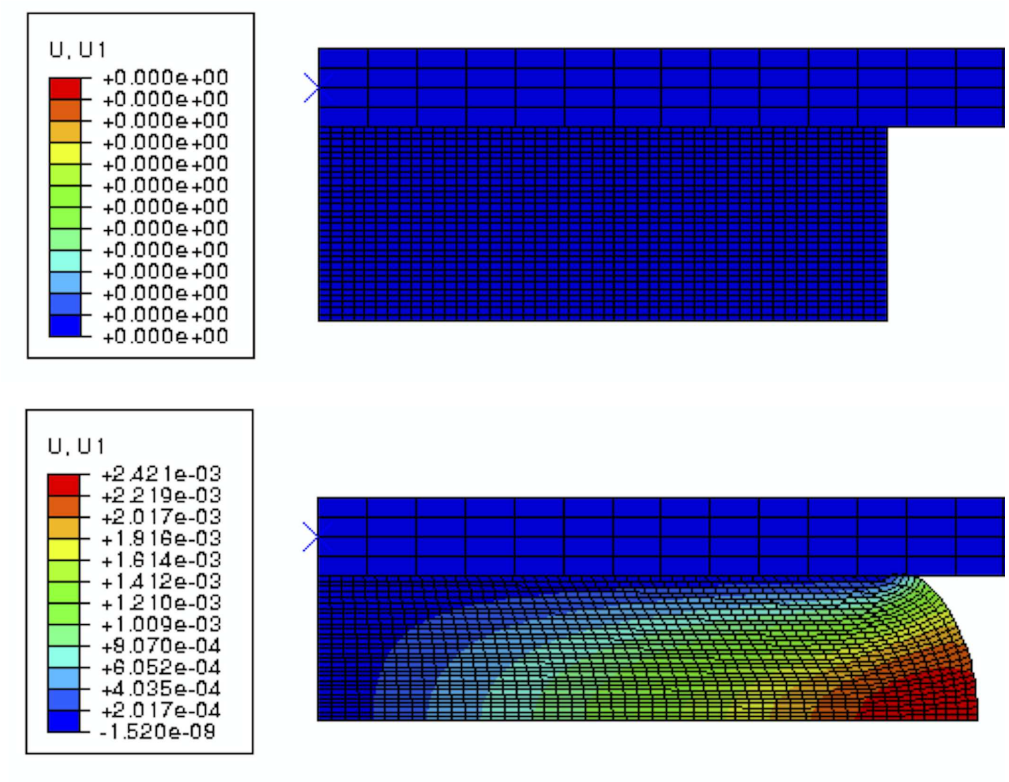

Figure 5: Axisymmetric FE model of cylindrical gelatin samples, compressed by a rigid body with tie constraints at the sample-plate interface to model the no-slip boundary condition. Only the top right quadrant of the specimen is modelled, exploiting symmetry about its midplane. Top: initial configuration. Bottom: following deformation. Contours indicate lateral displacement (metres).

3.5. Model results

The optimised model parameters are listed in Table 1, and the corresponding predicted load-displacement curves are shown in Fig. 6, the latter indicating a good fit to the experimental data. Importantly, the loading rate-dependence of the response appears to be captured well. The fit for all three curves is very good, but especially so for the 'medium' and 'fast' results.

Table 1: Optimised constitutive model parameter values

Parameter	μ_1	α_1	γ_1	τ_1
Estimated Value	11934 Pa	1.90	0.56	5.85 sec

3.5.1. Sensitivity analysis

A sensitivity analysis of the constitutive model parameters was performed to assess the reliability of the optimisation procedure. The values of each parameter were perturbed from their estimated optima by $\pm 1\%$ and the cost function was recomputed. The results are depicted in Fig. 7. It is readily seen that the cost function is highly sensitive to each parameter, with this small perturbation producing a cost function value change of $> 200\%$

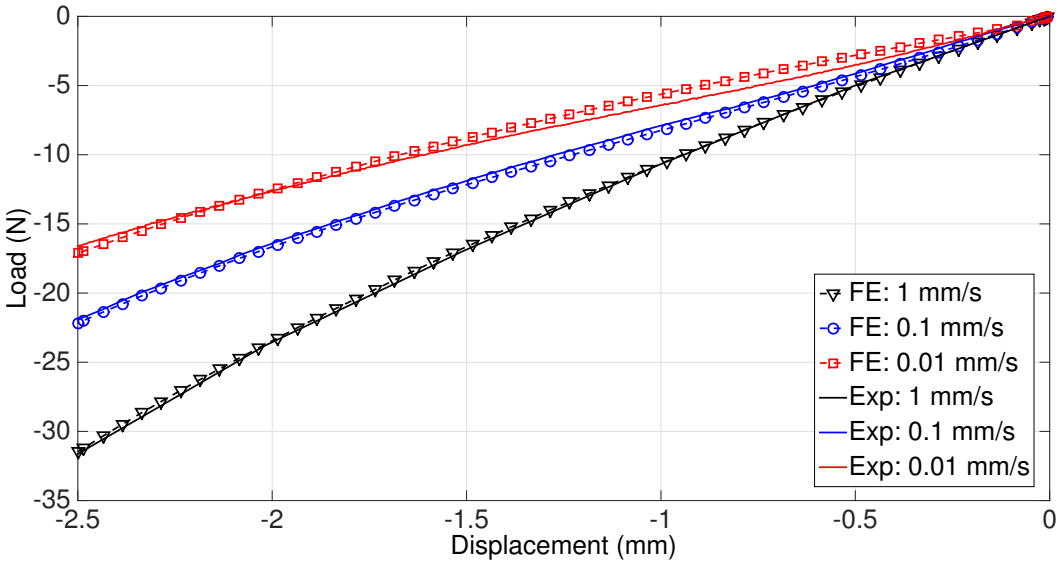

Figure 6: Model-predicted load-displacement curves using optimised parameters and mean experimental curves for all three loading rates.

in each case. From this, and the visually good fit shown in Fig. 6, which suggests erroneous local minima were avoided, we conclude that a reliable global optimal fit of the parameters was achieved using the procedure described above.

4. Discussion and conclusions

The main contribution of this study is formulation and experimental identification of a lightweight but flexible constitutive model for ballistic gelatin at quasi-static strain rates. The computational framework, together with the general form of the Ogden viscoelastic model, could also be employed to characterise the behaviour of a variety of soft tissues and soft tissue-substitutes in various applications. The proposed model captures both the finite strain characteristics and rate-dependence (for strain rates varying by two orders of magnitude) of the material's response in compression.

In previous studies (Kwon and Subhash (2010)), the increasing stiffness with strain rate was attributed to mechanisms like internal energy dissipation (related to underlying crosslinking/bond-structure of the gelatin) and hydrocluster formation (related to the microstructure of the gelatin). Though these were hypothesised to account for changes observed up to dynamic loading rates ($\sim 10^3 \mathrm{s}^{-1}$), they may also be applicable at the quasi-static rates considered here. These phenomena may also partially account for the variation in sample responses (though, as noted, this was not great), given that different samples, especially those from different preparation batches, would indeed contain variations in bond- and microstructure.

In our analysis of the experimental configuration, it was assumed that the specimen surfaces perfectly adhered to the loading plates. Visual inspection during the experiments gave no indication that this assumption was flawed, yet it cannot be proved conclusively. Some asymmetry of deformation is apparent, for example, in the images depicted in Fig.

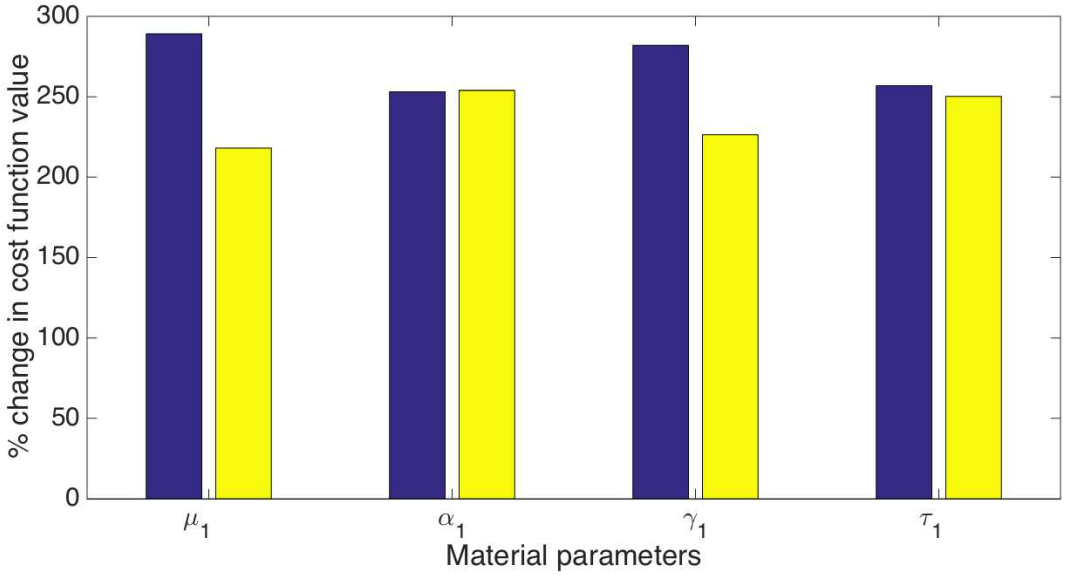

Figure 7: Sensitivity analysis of constitutive model parameters: percentage change of the cost function for a $\pm 1\%$ change in each material parameter, relative to their estimated optimal values. black and yellow bars show results of a 1% increase and decrease, respectively, in the relevant parameter.

3. The latter, however, may also be partially attributable to imperfections in the specimen shape, as a result of the manufacturing process. Either of these phenomena will inevitably introduce errors that are not easily quantifiable. Nevertheless, the high consistency of the results (evidenced by the relatively small standard deviations in Fig. 4) suggests that their effects, which may be expected rather to promote *in*consistency across samples, were small.

While our aim in this work was not to establish comparisons between the mechanical behaviour of gelatin and that of any particular tissue, such comparisons may inevitably be informative. Given that different strain energy formulations are used in different studies, the most straightforward means of comparing elastic properties is via the initial shear moduli μ_0, which may be computed from the parameters of the various formulations. For the single-term Ogden model used here, a value of $\mu_0 = \alpha_1\mu_1/2 \approx 11337$ Pa was obtained for gelatin. Samur et al. (2007), based on three in vivo experiments, and fitting to a Mooney-Rivlin model, obtained equivalent μ_0 values between 11716 Pa and 12476 Pa for porcine liver, which are remarkably close to our estimate for gelatin. For the viscoelastic model components, Samur et al. used a two-term Prony series, the parameters for which, unfortunately, are not easily comparable with those of our one-term formulation.

The material characterisation of ballistic gelatin presented here can find application in *in situ* studies that employ the material in physical phantoms (such as of breast, liver or brain) for surgical training (Malekzadeh et al. (2011)) or evaluation of traumatic brain injuries, and in *in silico* studies investigating computational models of such processes (Chafi et al. (2010)). The constitutive model and optimised material parameter values indicate that ballistic gelatin has similar properties to soft tissues in general, which is encouraging for its use as a soft tissue simulant.

5. Acknowledgements

This work was partially supported by the European Commission Framework Programme 7, Understanding Interactions of Human Tissue with Medical Devices (UNITISS, FP7-PEOPLE-2011-IAPP/286174). The authors are grateful to Dr. Gwendolen Reilly and The Kroto Research Institute, The University of Sheffield, for their guidance and co-operation and for providing access to experimental facilities.

6. References

Alley, M. D., Schimizze, B. R., Son, S. F., 2011. Experimental modeling of explosive blast-related traumatic brain injuries. Neuroimage 54, S45–S54.

Breeze, J., Hunt, N., Gibb, I., James, G., Hepper, A., Clasper, J., 2013. Experimental penetration of fragment simulating projectiles into porcine tissues compared with simulants. Journal of forensic and legal medicine 20 (4), 296–299.

Chafi, M., Karami, G., Ziejewski, M., 2010. Biomechanical assessment of brain dynamic responses due to blast pressure waves. Annals of biomedical engineering 38 (2), 490–504.

Cronin, D., 2011. Ballistic gelatin characterization and constitutive modeling. In: Dynamic Behavior of Materials, Volume 1. Springer, pp. 51–55.

Cronin, D., Falzon, C., 2009. Dynamic characterization and simulation of ballistic gelatin. In: 2009 SEM Conference & Exposition on Experimental & Applied Mechanics, June. pp. 1–4.

Cronin, D., Falzon, C., 2011. Characterization of 10% ballistic gelatin to evaluate temperature, aging and strain rate effects. Experimental mechanics 51 (7), 1197–1206.

Detwiler, P. W., Watkins, J. F., Rose, E. A., Ratner, A., Vu, L. P., Severinsky, J. Y., Rosenschein, U., 1991. Mechanical and acoustic analysis in ultrasonic angioplasty. In: SPIE. Vol. 1425. pp. 149–155.

Drury, J. L., Mooney, D. J., 2003. Hydrogels for tissue engineering: scaffold design variables and applications. Biomaterials 24 (24), 4337–4351.

Holzapfel, G., 2000. Nonlinear Solid Mechanics: A Continuum Approach for Engineering. John Wiley & Sons.

Holzapfel, G. A., 1996. On large strain viscoelasticity: continuum formulation and finite element applications to elastomeric structures. International Journal for Numerical Methods in Engineering 39 (22), 3903–3926.

Juliano, T. F., Forster, A. M., Drzal, P. L., Weerasooriya, T., Moy, P., VanLandingham, M. R., 2006. Multiscale mechanical characterization of biomimetic physically associating gels. Journal of materials research 21 (8), 2084–2092.

Kalcioglu, Z. I., Qu, M., Van Vliet, K. J., Strawhecker, K. E., VanLandingham, M. R., 2010. Multiscale characterization of relaxation times of tissue surrogate gels and soft tissues. In: 27th Army Science Conference Proceedings, Orlando, FL, November.

Kolling, S., Du Bois, P., Benson, D., Feng, W., 2007. A tabulated formulation of hyperelasticity with rate effects and damage. Computational Mechanics 40, 885–899.

Kwartowitz, D. M., 2012. Materials and polymers for use in surgical simulation and validation. Polymers for Vascular and Urogenital Applications, 223.

Kwon, J., Subhash, G., 2010. Compressive strain rate sensitivity of ballistic gelatin. Journal of biomechanics 43 (3), 420–425.

Lawrentschuk, N., Lindner, U., Klotz, L., 2011. Realistic anatomical prostate models for surgical skills workshops using ballistic gelatin for nerve-sparing radical prostatectomy and fruit for simple prostatectomy. Korean journal of urology 52 (2), 130–135.

Lindner, U., Lawrentschuk, N., Weersink, R. A., Raz, O., Hlasny, E., Sussman, M. S., Davidson, S. R., Gertner, M. R., Trachtenberg, J., 2010. Construction and evaluation of an anatomically correct multi-image modality compatible phantom for prostate cancer focal ablation. The Journal of urology 184 (1), 352–357.

Liu, L., Fan, Y., Li, W., 2014a. Viscoelastic shock wave in ballistic gelatin behind soft body armor. Journal of the mechanical behavior of biomedical materials 34, 199–207.

Liu, L., Jia, Z., Ma, X., Fan, Y., Li, W., Liu, H., 2014b. A spherical cavity expansion model of large elastic deformation and its application to ballistic gelatin penetration problems. International Journal of Impact Engineering 71, 106–116.

Maier-Hein, L., Walsh, C. J., Seitel, A., Hanumara, N. C., Shepard, J.-A., Franz, A., Pianka, F., Müller, S. A., Schmied, B., Slocum, A. H., et al., 2009. Human vs. robot operator error in a needle-based navigation system for percutaneous liver interventions. In: SPIE medical imaging. International Society for Optics and Photonics, pp. 72610Y–72610Y.

Malekzadeh, S., Pfisterer, M. J., Wilson, B., Na, H., Steehler, M. K., 2011. A novel low-cost sinus surgery task trainer. Otolaryngology–Head and Neck Surgery 145 (4), 530–533.

März, K., Franz, A., Seitel, A., Winterstein, A., Hafezi, M., Saffari, A., Bendl, R., Stieltjes, B., Meinzer, H.-P., Mehrabi, A., et al., 2014. Interventional real-time ultrasound imaging with an integrated electromagnetic field generator. International journal of computer assisted radiology and surgery, 1–10.

Mendez-Probst, C., Vanjecek, M., Razvi, H., Cadieux, P., 2010. Ordnance gelatine as an in vitro tissue simulation scaffold for extracorporeal shock wave lithotripsy. Urological research 38 (6), 497–503.

Miller, K., Chinzei, K., 2002. Mechanical properties of brain tissue in tension. Journal of biomechanics 35 (4), 483–490.

Miranda, D., Cristiano, K., Gutiérrez, J., 2013. Breast phantom for mammary tissue characterization by near infrared spectroscopy. In: Journal of Physics: Conference Series. Vol. 466. IOP Publishing, p. 012018.

Moy, P., Tusit, W., Gunnarsson, C., 2008. Tensile deformation of ballistic gelatin as a function of loading rate. In: Proceedings of the XIth International Congress and Exposition June. pp. 2–5.

Nicholas, N., Welsch, J., 2004. Institute for non-lethal defense technologies report: Ballistic gelatin. Tech. rep., DTIC Document.

Pervin, F., Chen, W. W., 2011. Mechanically similar gel simulants for brain tissues. In: Dynamic Behavior of Materials, Volume 1. Springer, pp. 9–13.

Richler, D., Rittel, D., 2014. On the testing of the dynamic mechanical properties of soft gelatins. Experimental Mechanics 54 (5), 805–815.

Robertson, D., Cook, D., 2014. Unrealistic statistics: How average constitutive coefficients can produce non-physical results. Journal of the mechanical behavior of biomedical materials 40, 234–239.

Roylance, D., 2001. Engineering viscoelasticity. Department of Materials Science and Engineering–Massachusetts Institute of Technology, Cambridge MA 2139, 1–37.

Salisbury, C., Cronin, D., 2009. Mechanical properties of ballistic gelatin at high deformation rates. Experimental mechanics 49 (6), 829–840.

Samur, E., Sedef, M., Basdogan, C., Avtan, L., Duzgun, O., 2007. A robotic indenter for minimally invasive measurement and characterization of soft tissue response. Medical Image Analysis 11 (4), 361–373.

Subhash, G., Kwon, J., Mei, R., Moore, D., 2012. Non-newtonian behavior of ballistic gelatin at high shear rates. Experimental mechanics 52 (6), 551–560.

Sun, J.-Y., Zhao, X., Illeperuma, W. R., Chaudhuri, O., Oh, K. H., Mooney, D. J., Vlassak, J. J., Suo, Z., 2012. Highly stretchable and tough hydrogels. Nature 489 (7414), 133–136.

Sutcliffe, J., Hardman, R. L., Dornbluth, N. C., Kist, K. A., 2013. A novel technique for teaching challenging ultrasound-guided breast procedures to radiology residents. Journal of Ultrasound in Medicine 32 (10), 1845–1854.

Swain, M., Kieser, D., Shah, S., Kieser, J., 2014. Projectile penetration into ballistic gelatin. Journal of the mechanical behavior of biomedical materials 29, 385–392.

Taylor, Z. A., Comas, O., Cheng, M., Passenger, J., Hawkes, D. J., Atkinson, D., Ourselin, S., 2009. On modelling of anisotropic viscoelasticity for soft tissue simulation: Numerical solution and gpu execution. Medical Image Analysis 13 (2), 234–244.

Taylor, Z. A., Kirk, T. B., Miller, K., 2007. Confocal arthroscopy-based patient-specific constitutive models of cartilaginous tissues - II: prediction of reaction force history of meniscal specimens. Computer Methods in Biomechanics and Biomedical Engineering 10 (5), 327–336.

Trexler, M., Lennon, A., Wickwire, A., Harrigan, T., Luong, Q., Graham, J., Maisano, A., Roberts, J., Merkle, A., 2011. Verification and implementation of a modified split hopkinson pressure bar technique for characterizing biological tissue and soft biosimulant materials under dynamic shear loading. Journal of the mechanical behavior of biomedical materials 4 (8), 1920–1928.